We are IntechOpen,
the world's leading publisher of
Open Access books
Built by scientists, for scientists

4,800
Open access books available

122,000
International authors and editors

135M
Downloads

Our authors are among the

154
Countries delivered to

TOP 1%
most cited scientists

12.2%
Contributors from top 500 universities

CLARIVATE ANALYTICS
BOOK
CITATION
INDEX
INDEXED

WEB OF SCIENCE™

Selection of our books indexed in the Book Citation Index
in Web of Science™ Core Collection (BKCI)

Interested in publishing with us?
Contact book.department@intechopen.com

Turbulent Flow and Heat Transfer Characteristics of a Micro Combustor

Tae Seon Park[1] and Hang Seok Choi[2]
[1]School of Mechanical Engineering, Kyungpook National University
[2]Environment & Energy Systems Research Division,
Korea Institute of Machinery and Materials
Republic of Korea

1. Introduction

Currently, a micro gas turbine (MGT) has been widely drawing attention as a distributed energy generation system for an individual household or a small community. In parallel to the progress of MGT technology, a fuel cell has been highlighted for its high efficiency and environmental advantages. For MGT, its efficiency can reach to 40% (Mcdonald, 2000), but it seems to be difficult to achieve higher efficiency than 40% (Kee et al., 2005; Suzuki et al., 2000). However, the efficiency of solid oxide fuel cell (SOFC) for electricity generation recently becomes 50% or higher. Therefore, a hybrid system with MGT and SOFC is promising because the MGT/SOFC hybrid system can provide higher efficiency over 70% (Massardo & Lubelli, 2000). Recently, (Suzuki et al., 2000) proposed the MGT/SOFC hybrid system having a micro combustor. In their system, the micro combustor is an important component to realize high system efficiency and low toxic exhausted gas. In a combustor of that kind, combustion efficiency may decrease by two critical issues, because combustion in a very small chamber may not simply resemble a scaled-down version of its large-scale counterpart (Choi & Park, 2009).

One is the incomplete mixing between oxidant and fuel, which is highly related to reliable ignition and flammable limits. As a combustor size decreases, Reynolds number becomes smaller. Such a small combustor may be suffering from incomplete mixing between fuel and oxidant, insufficient fuel residence time for complete combustion and high heat transfer rate to combustor outside because of high surface to volume ratio. In that situation, flow field is significantly stabilized by viscous effect and this may restrain active turbulent mixing. This mechanism is not favorable for small combustor. Therefore, mixing enhancement is a critical consideration to develop such a micro combustor. (Suzuki et al., 2000) suggested a baffle plate to enhance the slow mixing in low Reynolds number condition. Its effectiveness is evaluated by the succeeding studies by (Choi et al., 2001; Choi et al., 2005; Choi et al., 2006a; Choi et al., 2008) for turbulent mixing fields downstream of the baffle plate. Micro combustor of this type is expected to secure zero emission of toxic gases and to maintain a stable flame for burning the effluent of SOFC in an extraordinary fuel lean condition.

The other issue is the effect of heat loss to wall. This may be ignored in a large-scale combustor, but it is an important factor to a micro combustor. Heat generation depends on the combustor volume and mixing characteristics, while the heat loss is proportional to the surface area. In general, the surface-to-volume ratio for a micro combustor is larger than that

of a large-scale counterpart. For a can-type combustor, combustor volume and surface area are $V = \pi r^2 L$ and $A = 2\pi r L$, respectively. Here, r and L are radius and length of the combustor. Therefore, the heat loss increases more rapidly than the heat generation as the combustor size is reduced. As discussed by (Choi et al., 2001; Choi et al., 2006b), a heat loss has a critical influence on combustor efficiency. Excess enthalpy loss makes it difficult to sustain stable combustion by thermal quenching.

This chapter provides characteristics of turbulent flow and heat transfer in a micro can combustor (Choi et al., 2001; Choi et al., 2005; Choi et al., 2006a; Choi et al., 2006b; Choi et al., 2008; Choi et al., 2009). Three different shapes of baffle plates, leading to different values of oxidant to fuel velocity ratios, are selected and thermal quantities are scrutinized based on the flow structures. In particular, we are focused on investigating the heat loss of nonreacting flows in the micro combustor with baffle plate. For that purpose, conjugate heat transfer of the combustor is analyzed by using large eddy simulation (LES). As a result, peculiar characteristics of the heat transfer in the micro combustor with multiple jet flows are elucidated.

2. Numerical methods

2.1 Computational procedure

In LES method, small-scale or subgrid-scale quantities of governing equations are filtered out and then comparably large-scale ones are considered. The filtered forms of continuity and momentum equations for incompressible fluid are expressed as follows:

$$\frac{\partial \overline{u}_i}{\partial x_i} = 0, \tag{1}$$

$$\frac{\partial \overline{u}_i}{\partial t} + \overline{u}_j \frac{\partial \overline{u}_i}{\partial x_j} = -\frac{1}{\rho}\frac{\partial \overline{p}}{\partial x_j} - \frac{\partial \tau_{ij}}{\partial x_j} + \nu \frac{\partial^2 \overline{u}_i}{\partial x_j \partial x_j}, \tag{2}$$

where $\overline{u}_i$, $\overline{p}$ and $\overline{\tau}_{ij}$ are the filtered velocity, filtered pressure and the subgrid-scale stress tensor, respectively. In Equation (2), $\overline{\tau}_{ij}$ is defined as $\overline{\tau}_{ij} \equiv \overline{u_i u_j} - \overline{u}_i \overline{u}_j$ and the dynamic subgrid-scale model (Lilly, 1992) is adopted in the present study as follows:

$$\overline{\tau}_{ij} - 1/3\delta_{ij}\overline{\tau}_{kk} = -2\nu_t \overline{S}_{ij} \tag{3}$$

here $\overline{S}_{ij} = 0.5(\partial \overline{u}_i / \partial x_j + \partial \overline{u}_j / \partial x_i)$ and ν_t is the eddy viscosity to be obtained. The eddy viscosity is given by $\nu_t = C\overline{\Delta}^2 |\overline{S}|$ and $|\overline{S}| = \sqrt{2\overline{S}_{ij}\overline{S}_{ij}}$. Here, the width of grid filter is taken by $\overline{\Delta} = (\Delta x \Delta y \Delta z)^{1/3}$ and model constant C is obtained from the least square technique suggested by (Lilly, 1992).

For turbulent thermal field, the filtered governing equation of temperature, $\overline{\theta}$, is used to represent the evolution of thermal field.

$$\frac{\partial \overline{\theta}}{\partial t} + \overline{u}_j \frac{\partial \overline{\theta}}{\partial x_j} = \frac{\partial}{\partial x_j}\left[\frac{\nu}{\mathrm{Pr}}\frac{\partial \overline{\theta}}{\partial x_j} - \frac{\nu_t}{\mathrm{Pr}_t}\frac{\partial \overline{\theta}}{\partial x_j} \right], \tag{4}$$

here Pr_t is turbulent Prandtl number and its value is carefully selected (Moin et al., 1991; Andreopoulos, 1993). The Prandtl numbers are set constant as $Pr = 0.7$ and $Pr_t = 0.9$. Although more resonable value is possible, it is not important because this study aims to see how the geometrical variation is effective on the heat transfer variation.

The $k - \varepsilon - f_\mu$ model of (Park et al., 2003) is employed for comparison. The turbulent kinetic energy equation and its dissipation rate equation are

$$\frac{\partial k}{\partial t} + U_j \frac{\partial k}{\partial x_j} = \frac{\partial}{\partial x_j}\left[\left(\nu + \frac{\nu_t}{\sigma_k}\right)\frac{\partial k}{\partial x_j}\right] + P_k - \varepsilon, \tag{5}$$

$$\frac{\partial \varepsilon}{\partial t} + U_j \frac{\partial \varepsilon}{\partial x_j} = \frac{\partial}{\partial x_j}\left[\left(\nu + \frac{\nu_t}{\sigma_\varepsilon}\right)\frac{\partial \varepsilon}{\partial x_j}\right] + (C_{\varepsilon 1}^* P_k - C_{\varepsilon 2} f_2 \varepsilon)/T + C_{\varepsilon 3}(1 - f_W)\nu\nu_t\left(\frac{\partial^2 U_i}{\partial x_j \partial x_k}\right)^2. \tag{6}$$

Here, $f_2 = 1 - (2/9)\exp(-0.33R_t^{1/2})$, $T = \sqrt{(k/\varepsilon)^2 + 36(\nu/\varepsilon)}$
and $C_{\varepsilon 1}^* = 1.42 + C_\mu /(1 + 5f_{\mu 2}(C_\mu \eta)^2)$.

The Reynolds stress can be expressed in a conventional form as

$$-\overline{u_i u_j}^{linear} = \nu_t\left(\frac{\partial U_i}{\partial x_j} + \frac{\partial U_j}{\partial x_i}\right) - \frac{2}{3}k\delta_{ij}, \tag{5}$$

$$-\overline{u_i u_j} = -\overline{u_i u_j}^{linear} - k\beta_2\left(S_{ik}^* S_{kj}^* - \frac{1}{3}S^{*2}\delta_{ij}\right) - k\beta_3\left(W_{ik}^* S_{kj}^* - S_{ik}^* W_{kj}^*\right) \tag{6}$$

$$-k\beta_4\left(S_{il}^* S_{lm}^* W_{mj}^* - W_{il}^* S_{lm}^* S_{mj}^*\right) - k\beta_5\left(W_{il}^* W_{lm}^* S_{mj}^* - S_{il}^* W_{lm}^* W_{mj}^* + 0.5S_{ij}^* W^{*2} - \frac{2}{3}III_S\delta_{ij}\right),$$

where $\nu_t = C_\mu f_\mu k^2 /\varepsilon$, $\beta_2 = \tilde{\beta}_2 + \tilde{\beta}_{2,wall}C_W$, $\beta_3 = \tilde{\beta}_3 + \tilde{\beta}_{3,wall}C_W$, $\beta_4 = \tilde{\beta}_4$, $\beta_5 = \tilde{\beta}_5$, $III_S = S_{lm}^* W_{mn}^* W_{nl}^*$, $S_{ij}^* = S_{ij}k/\varepsilon$, $W_{ij}^* = W_{ij}k/\varepsilon$, $S^* = \sqrt{2S_{ij}^* S_{ij}^*}$, $W^* = \sqrt{2W_{ij}^* W_{ij}^*}$. In the above, β_i represents the strain dependent coefficients and the model constant is set as $C_W = 1$ for $i = j$ and $C_W = 0$ for $i \neq j$. Further details regarding the formulation of the nonlinear stress-strain relation can be found in (Park et al., 2003). The variations of the eddy viscosity are allowed by decomposing f_μ into two parts, i.e., $f_\mu = f_{\mu 1}f_{\mu 2}$, where $f_{\mu 1}$ signifies the effect of wall-rpoximity in the near-wall region while $f_{\mu 2}$ represents the strain effects.

$$f_{\mu 1} = (1 + f_D R_t^{-3/4})f_W^2, \quad \frac{\partial^2 f_W}{\partial x_j \partial x_j} = \frac{R_t^{3/2}}{8.4^2 L^2}(f_W - 1) \tag{7}$$

$$f_{\mu 2} = \frac{5(1 + g)}{g^2 + C_\mu g^3 + A_S}, \tag{8}$$

$$g = \begin{cases} \dfrac{C_0}{3} + (P_1 + \sqrt{P_2})^{1/3} + \sin(P_1 - \sqrt{P_2}) \mid P_1 - \sqrt{P_2} \mid^{1/3} & P_2 \geq 0 \\[3mm] \dfrac{C_0}{3} + 2(P_1^2 - P_2)^{1/6} \cos\left[\dfrac{1}{3} \arccos\left(\dfrac{P_1}{\sqrt{P_1^2 - P}} \right) \right] & P_2 < 0 \end{cases} \tag{9}$$

$$P_1 = C_0\left[\frac{C_0^2}{27} - \frac{(A_S - \alpha_1 \eta^2)}{6} + \frac{1}{2} \right], \quad P_2 = P_1^2 - \left[\frac{C_0^2}{9} - \frac{(A_S - \alpha_1 \eta^2)}{3} \right] \tag{10}$$

Here, $f_D = 10\exp[-(R_t/120)^2]$, $L^2 = k^3/\varepsilon^2 + 70^2\sqrt{v^3/\varepsilon}$, $A_S = \alpha_3^2\xi^2 - \alpha_2^2\eta^2/3$, $\eta = f_W S^*$ and $\xi = f_W W^*$. The model constants are set as $C_\mu = 0.09$, $C_0 = 2.5$, $\alpha_1 = 0.48$, $\alpha_2 = 0.375$, $\alpha_3 = 0.8$, $\sigma_k = 1.1$, $\sigma_\varepsilon = 1.3$, $C_{\varepsilon 2} = 1.9$ and $C_{\varepsilon 3} = 0.8$.

For the time integration of the governing equations, a PISO(Pressure Implicit with Splitting of Operator) algorithm (Issa, 1986) is adopted to Eqs. (1) through (4). Details regarding the solution procedure of the PISO algorithm can be found in (Issa, 1986) and (Park, 2006a; Park, 2006b). For the spatial discretization of the governing equations, the fourth-order COMPACT scheme (Lele, 1992) is used for the convective terms of the equations, and the fourth-order central differencing scheme is applied to the diffusion and other remaining terms. In the present study, a non-staggered grid is adopted in the generalized coordinate system. Therefore, to avoid the pressure-velocity decoupling a momentum interpolation technique is employed. The numerical method used in the present LES is fully validated as discussed in (Park, 2006a; Park, 2006b) for the turbulent channel flows and for a turbulent jet flow by (Choi et al., 2006a).
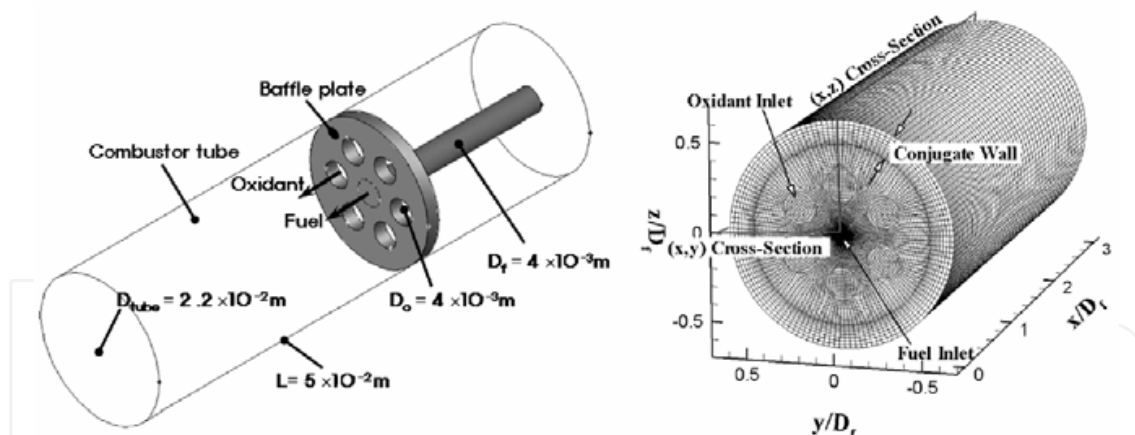

Fig. 1. A proposed micro combustor for case A. (a) configuration and (b) grid

2.2 Computational conditions

Figure 1 shows the configuration of the micro combustor, its computational domain and grid system, respectively and Table 1 describes calculation conditions for each baffle plate shape (Choi et al., 2008; Choi & Park 2009). In Fig. 1 (a), an injection nozzle for fuel is located in the center of the baffle plate and it is surrounded by six oxidant injection holes. The geometrical dimensions of the combustor are illustrated in Fig. 1 (a) for the case A. As shown in Table 1, velocity ratio is varied with the same baffle geometry or the diameter ratio, D_o/D_f, is changed so that the oxidant to fuel velocity ratio V_o/V_f is also changed. In the cases of A1, A2

and A3, Reynolds number is maintained in a similar level with the identical geometry, which is based on the total gas flow rate and the inner tube diameter of micro combustor, D_{tube}. On the other hand, Re_{tube} is kept constant as $\mathrm{Re}_{tube} = 3060$ for cases A2, B and C with different baffle plate configurations. This means that each flow rate for fuel and oxidant is kept constant but their velocities are changed. In Fig. 1 (b), x, y and z axes correspond to streamwise, transverse and spanwise directions, respectively for case A and the grid system consists of inner fluid and outer wall grids to solve conjugate heat transfer. The total grid number is set as $55 \times 52 \times 127$ through grid dependency test for all the cases of Table 1.

Case	D_o / D_f	V_o / V_f	Re_{tube}	$\theta_{inlet}(K)$	$\theta_{baffle}(K)$	$h_{tube}(W / m^2 K)$
A1	1	1.4	3,147	800	300	20
A2	1	2	3,060	800	300	20
A3	1	2.8	2,981	800	300	20
B	2	0.5	3,060	800	300	20
C	0.5	8	3,060	800	300	20

Table 1. Calculation condition

Figure 2 shows the spectra of scalar fluctuation (E_f) for case A2 having grid numbers of $55 \times 52 \times 127$ and three different spectra along the streamwise direction are presented at a center point between fuel and oxidant jets. In fully-resolved LES results, the general relation of the energy spectrum is well reproduced by the present LES. The result shows that the spatial filtering cutoff lies outside the inertial range and higher frequency region representing scalar dissipation (Peng & Davision, 2002) is also resolved. Hence, it can be judged indirectly from the figure that the present grid allocation is enough for LES study.
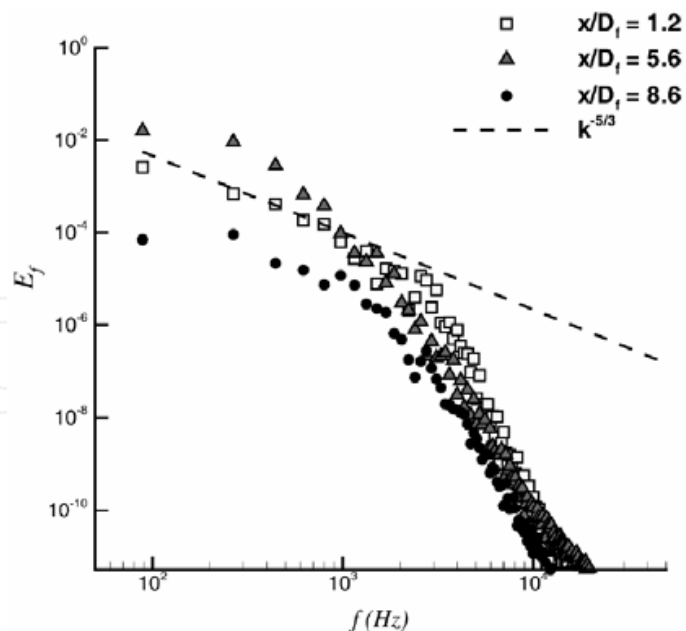

Fig. 2. Spectra of scalar fluctuation for case A2

Now, boundary conditions will be discussed as follows. For inlet boundary condition, three dimensional, unsteady nature of turbulence is considered as superposing random perturbation on streamwise velocity component as follows:

$$u = U_{inlet}(1 + I\Phi) \qquad (11)$$

here Φ is a probability function which returns real number randomly in the range of $-1 \leq \Phi \leq 1$ and I is the fluctuation intensity. U_{inlet} is the fuel or oxidant inlet velocity described in Table 1 as V_f or V_o. For the temperature, the Dirichlet condition is applied to the fuel and oxidant inlets, respectively as presented in Table 1. For outlet boundary conditions, convective boundary condition is used as follows.

$$\frac{\partial u_i}{\partial t} + U_{exit} \frac{\partial u_i}{\partial x_j} = 0 \qquad (12)$$

where U_{exit} is the mean velocity over the outflow boundary, and this convective boundary condition fulfils a correction on the streamwise velocity to ensure the global mass balance for mass flux of inlet and outlet boundaries (Ferziger & Peric, 2002). For temperature outlet boundary condition, the Neumann condition, $\partial\theta / \partial x = 0$, is adopted. In the wall boundary condition, no-slip and non-permeable conditions are adopted and for temperature the Dirichlet condition described in Table 1 is used for baffle plate. For the outer wall of combustor tube, a convective heat transfer boundary condition is applied and the heat transfer coefficient is set as in Table 1 considering the maximum limit of free convection of air. For the consistency condition of a fluid-solid interface to calculate conjugate heat transfer, the continuity of instantaneous temperature and heat flux is obtained as follows:

$$\theta|_f = \theta|_s \, , \; \kappa_f \left(\frac{\partial\theta}{\partial n} \right)_f = \kappa_s \left(\frac{\partial\theta}{\partial n} \right)_s \qquad (13)$$

here subscripts f and s mean fluid and solid region at the interface and n represents the wall-normal direction.
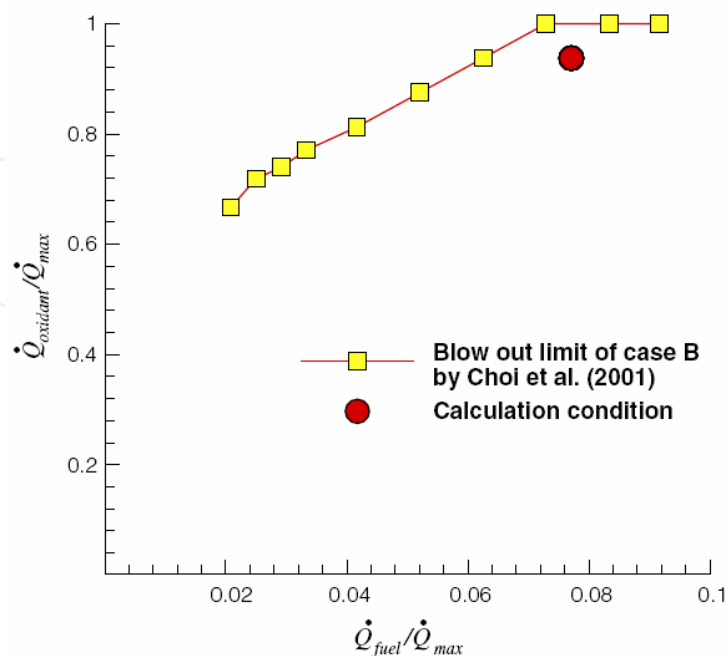

Fig. 3. Blowout limit of the flame in a micro can combustor in case B

To determine calculation condition for the mass flow rate of fuel and oxidant, experimental results (Choi et al., 2001) are used as follows. Figure 3 shows the blowout limit (Choi et al., 2001) of the flame experimentally obtained in a micro combustor with baffle plate B specified in Table 1. In case B, the mixing rate and flame stability are lower than those of other two cases. In the figure, $\dot{Q}_{oxidant}$ and $\dot{Q}_{fuel}$ mean the total volume flow rates of the oxidant and fuel which are entering into the combustor, respectively. The $\dot{Q}_{max}$ indicates the maximum volume flow rate of oxidant below which blowout of the flame does not occur and its value is $\dot{Q}_{max} = 8.0 \times 10^{-4} m^3 / s$.
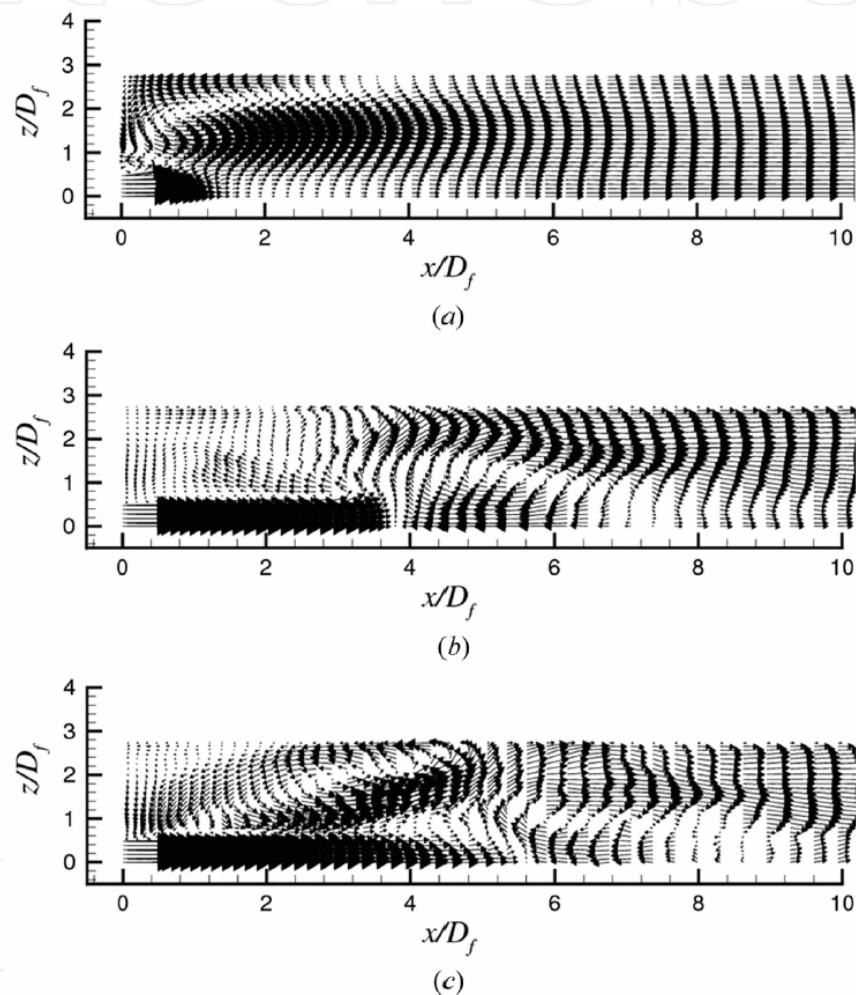
Fig. 4. Comparison of velocity vector map at (x, z) cross-section for case A2. (a) $k-\varepsilon$ model; (b) $k-\varepsilon-f_{\mu}$ model; and (c) the present LES

Figure 4 shows the comparison between the time-averaged results located at (x, z) plane of y = 0 obtained by using turbulence models and LES. Here, the fuel jet center is located at $x/D_f = 0$, $z/D_f = 0$, and the combustor wall is located along the top of the figure. For turbulence models, the standard $k-\varepsilon$ model and Park and Sung's low Reynolds number $k-\varepsilon-f_{\mu}$ one (Park et al., 2003) are used. In the case of the $k-\varepsilon$ model, the recirculation region between the fuel jet and wall appears but it cannot predict another flow recirculation region located in front of the fuel jet. However, the $k-\varepsilon-f_{\mu}$ model and LES predict the

flow recirculation region in front of the fuel jet but its size and location are different each other. Generally, for turbulence models it is hard to predict the turbulent flow fields with high fidelity having both free shear flow and wall bounded one according to its historical development. However, theoretically it is possible for LES to decompose the turbulence scale larger than the selected spatial filter (Benard & Wallace, 2002). Hence, in the present study, LES is selected to elucidate the turbulent and thermal fields of the micro combustor more accurately compared with turbulence models

3. Results and discussions

In the previous studies (Choi et al., 2005; Choi et al., 2006a; Choi et al., 2008), the characteristics of turbulent flow and turbulent mixing in confined multiple jet flows of a micro can combustor have been fully investigated for cases A2, B, and C by LES. It was proven that to control the fuel and oxidant jet velocities by the baffle geometry was very effective and practical for mixing in such a small combustor (Choi et al., 2001).
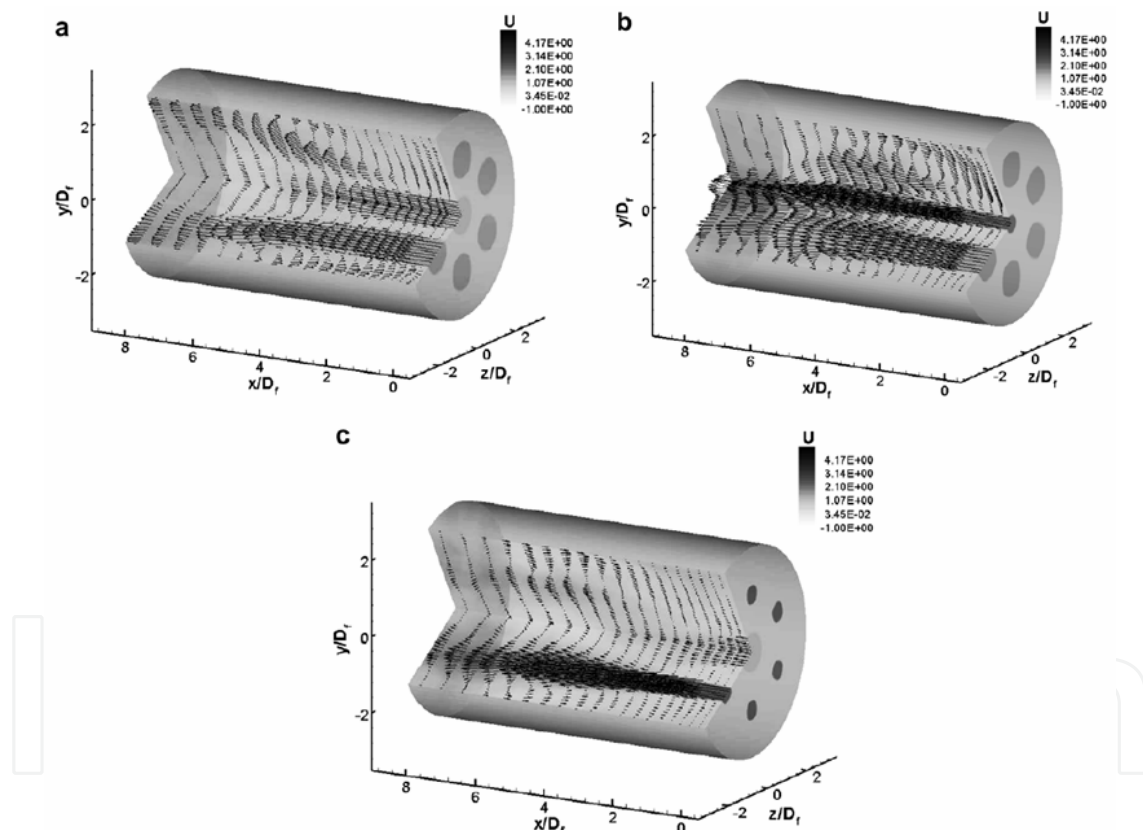
Fig. 5. Contour of streamwise velocity and velocity vector map in the two cross-sectional planes. (a)Case A2; (b) Case B; and (c) Case C

Figure 5 represents the vector map of time-averaged velocity and contour of time-averaged streamwise velocity in two different crosssectional planes for the three different baffle plate cases. This result explains the effect of baffle plate geometry on time-averaged velocity field. The upper cross-section shows the results in a plane slicing the middle of the space between the neighboring oxidant jets and the lower one shows the results in a plane slicing the center of a oxidant hole. In the figures, the magnitude of the velocity is non-dimensionalized by

fuel inlet velocity V_f of case A2. In all the three cases, large flow recirculation regions appear near the combustor wall, namely both between fuel jet and wall and between air jet and wall. These flow recirculation regions are called as near-wall flow recirculation regions in the following and the near-wall flow recirculation regions can be affected by the shape of baffle plate geometry like the one appearing downstream a backward facing step (Le et al., 1997). Peculiarity of the flow fields observed in two cases A and C is that, in addition to the near-wall flow recirculation regions, another flow recirculation region is formed downstream the fuel jet core region. This flow recirculation region is hereafter called as central flow recirculation region. This vortical flow can affect the mixing fields and actually is a key element of the enhanced mixing as will be discussed later. It may be worth to note that the central flow recirculation region is not found in case B. The central flow recirculation region ahead of the fuel jet originates from the lowering of fuel jet momentum due to the entrainment of fuel jet fluid into air jet.
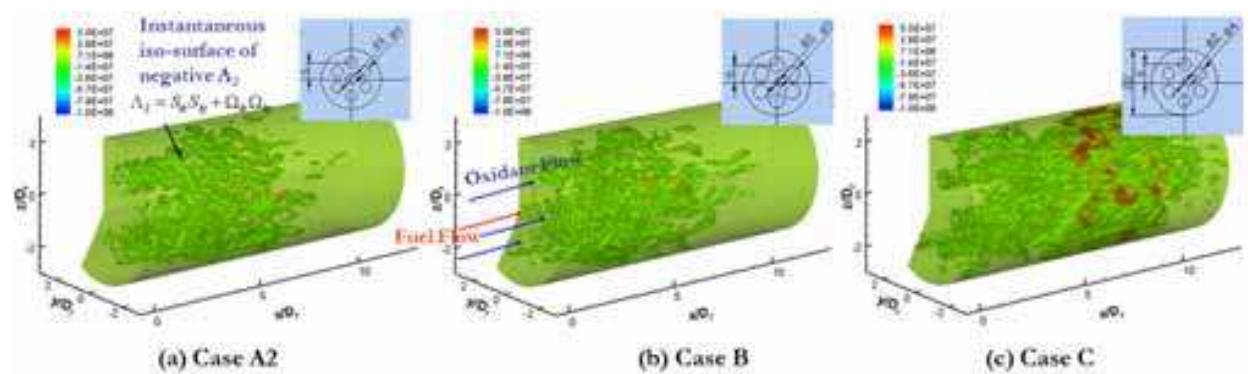
Fig. 6. Visualization of instantaneous vortices generated in the micro combustor

Figure 6 shows the iso-surfaces of instantaneous negative Λ_2 value captured at an instant. As can be seen in the figure, the generation of ring vortices is noticeable in the brim of oxidant jets and they develop downstream and interact with each other., i.e. between neighboring vortices or between ring vortices and fuel jets. This vortical flow makes the flowfield more turbulent and significantly enhances the heat transport.

Figure 7 shows the contours of turbulent kinetic energy $k = 0.5(\overline{u_i' u_i'})$ in (y,z) cross-sectional planes at different streamwise positions for case A. As observed in Fig. 7a, higher turbulent regions are limited at the edge of each oxidant jet and of ring shape at the first two locations downstream the baffle plate. These regions overlap the regions where the appearance of ring vortex is identified in Fig. 6a, which means that the shear layer caused by the vortices may affect the turbulent kinetic energy. This distribution pattern of turbulent kinetic energy is vaguely still observed at $x / D_f = 5.5$ in Fig. 7c. Mixing and dissipation of turbulence proceed toward downstream. Turbulent kinetic energy is now lowered and distributes almost uniformly in the cross-section at $x / D_f = 7.5$. This suggests that mixing of the scalar quantity is almost completed at this position.

Now, heat loss will be discussed by analyzing conjugate heat transfer of the combustor numerically. It is noted that the (x,z) cross-sectional plane is slicing the middle of the fuel and oxidant nozzles as shown in Fig. 1, so the vigorous interaction between the oxidant jet and fuel jet or wall may be displayed clearly comparing with other cross-sectional plane containing only fuel jet flow. This can be found in Fig. 8. Accordingly, in the following figures, the only (x,z) cross-sectional plane will be presented.
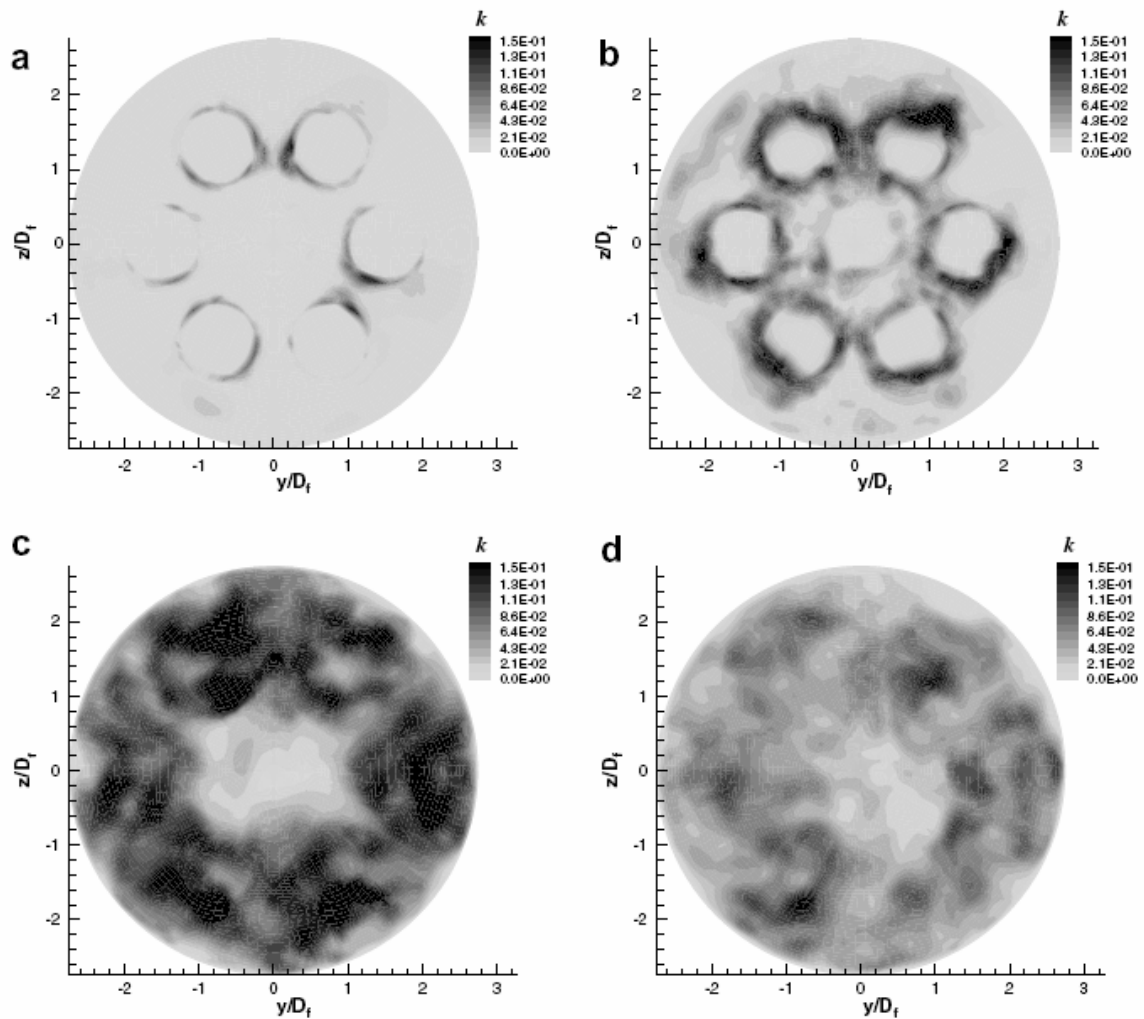
Fig. 7. Contour of turbulent kinetic energy at four different streamwise positions in case A2. (a) $x / D_f = 1.0$; (b) $x / D_f = 2.5$; (c) $x / D_f = 5.5$; and (d) $x / D_f = 7.5$
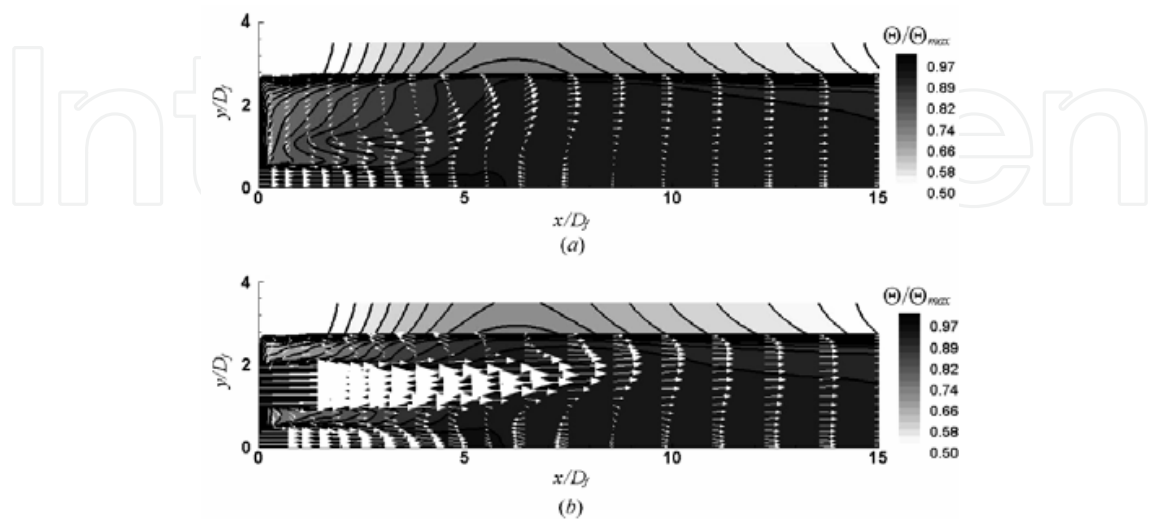

Fig. 8. Temperature contours with velocity vector map for case A2. (a) (x, y) cross-sectional plane and (b) (x, z) cross-sectional plane
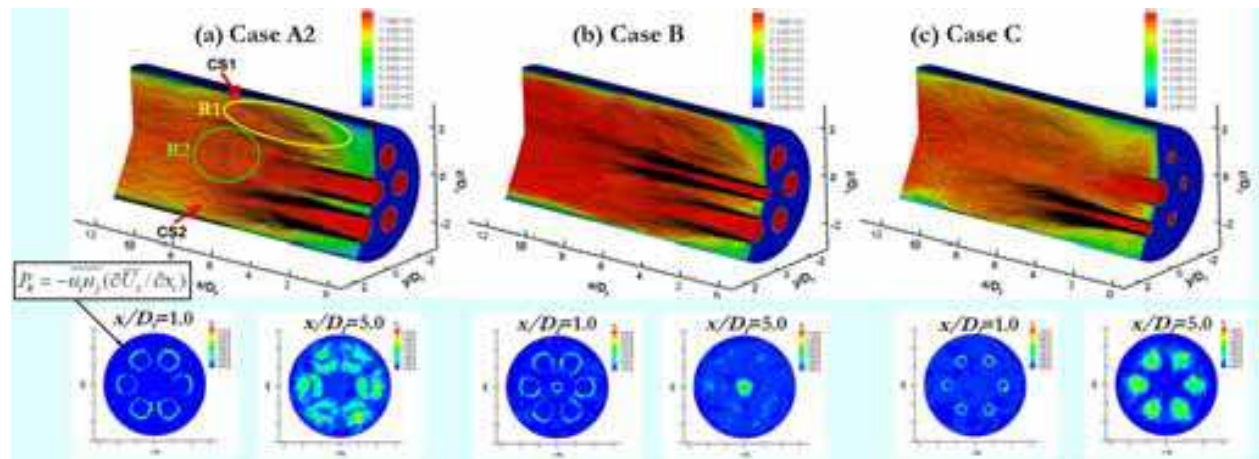
Fig. 9. Contours of time mean temperature, streamwise velocity and turbulent production
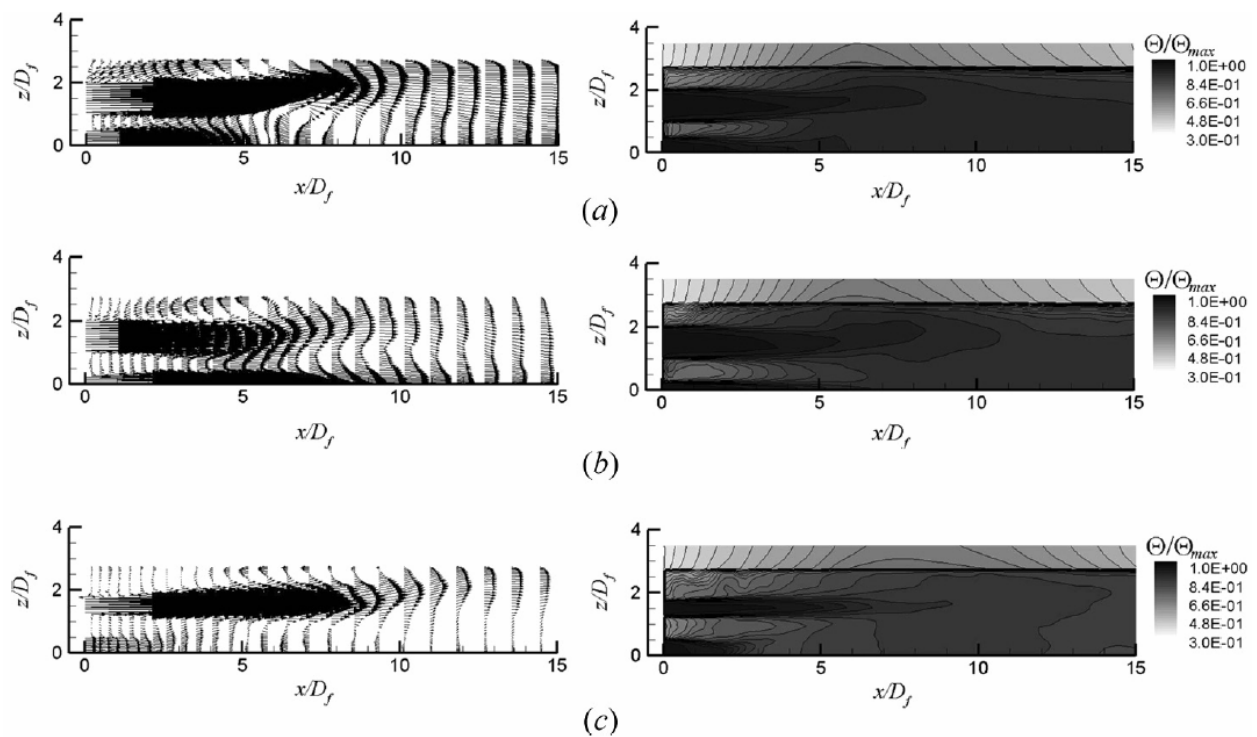

Fig. 10. Contour of Θ/Θ_{max} and velocity vector fields at (x, z) cross-sectional plane. (a) Case A2; (b) case B; and (c) case C

Figure 9 shows contours of the time averaged temperature, streamwise velocity and turbulent production and the time averaged temperature and velocity vector fields are shown in Fig. 10. In the figures, two large vortical regions exist as discussed (Choi et al., 2008) and these are called as near-wall recirculation region and central recirculation region, respectively. It is noted that near-wall recirculation region appears between combustor tube wall and jet flows and central one is located in front of fuel jet flow downstream the baffle plate. The near-wall recirculation region appears in all the three cases and the central recirculation one is generated only in the cases A2 and C. The streamlines of the flows are different according to the dissimilar recirculation regions and these flow fields affect the

transport of the passive scalar, i.e. temperature. The steep temperature gradient region close to the tube wall is located around $x/D_f = 6$ for the cases A2 and B and $x/D_f = 8$ for the case C, where the distinct upward flow motion to the wall exists by near-wall recirculation region. Recirculation zone (R1) carries hot fluids from the jets onto the cooler wall, where temperature gradient becomes steeper resulting in high Nusselt number. Recirculation zone (R2) pumps up the cooler fluids near wall mixing them well with hot fluids from the jet.
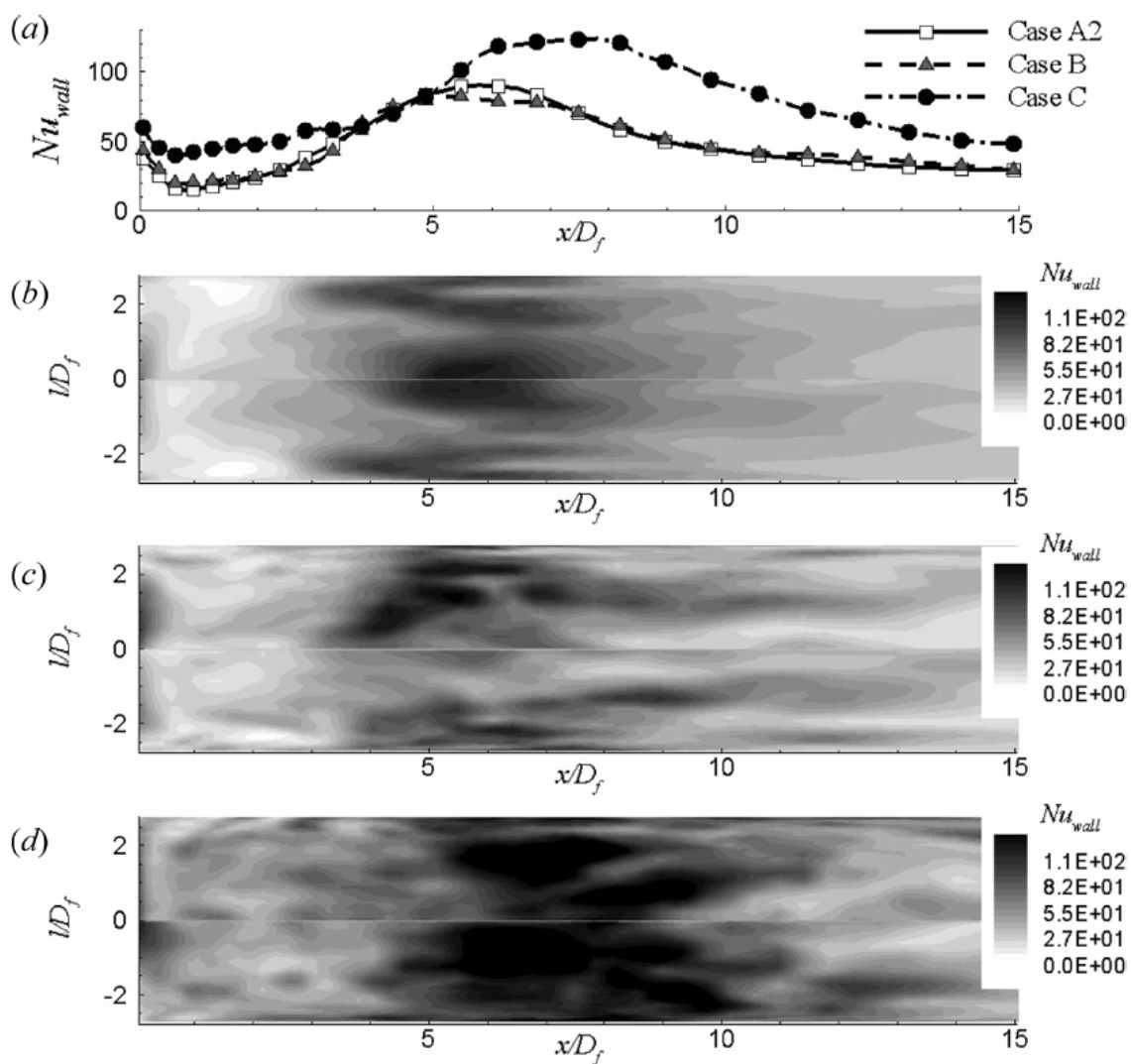
Fig. 11. Distributions of Nuwall along the streamwise direction. (a) Time and space averaged Nuwall; (b) case A2; (c) case B; and (d) case C

To analyze the effect of geometrical variations to the wall heat transfer, Nusselt number is displayed in Fig. 11. In Fig. 11 (a), the wall Nusselt number is averaged for time and space along the circumferential direction. As can be seen, the peak Nu_{wall} of the case C is the highest among the three cases. However, the wall heat transfer of the cases A2 and B is nearly same over the whole region. It is generally accepted that the evolution of a passive scalar is closely linked to the characteristics of the flow field. Therefore, the variation of the near-wall recirculation region can be considered as the source of the above Nu_{wall} feature.

This result suggests that the heat loss of the micro combustor with the baffle plate geometry depends on the baffle diameter ratio (D_o / D_f) and the oxidant to fuel velocity ratio (V_o / V_f).
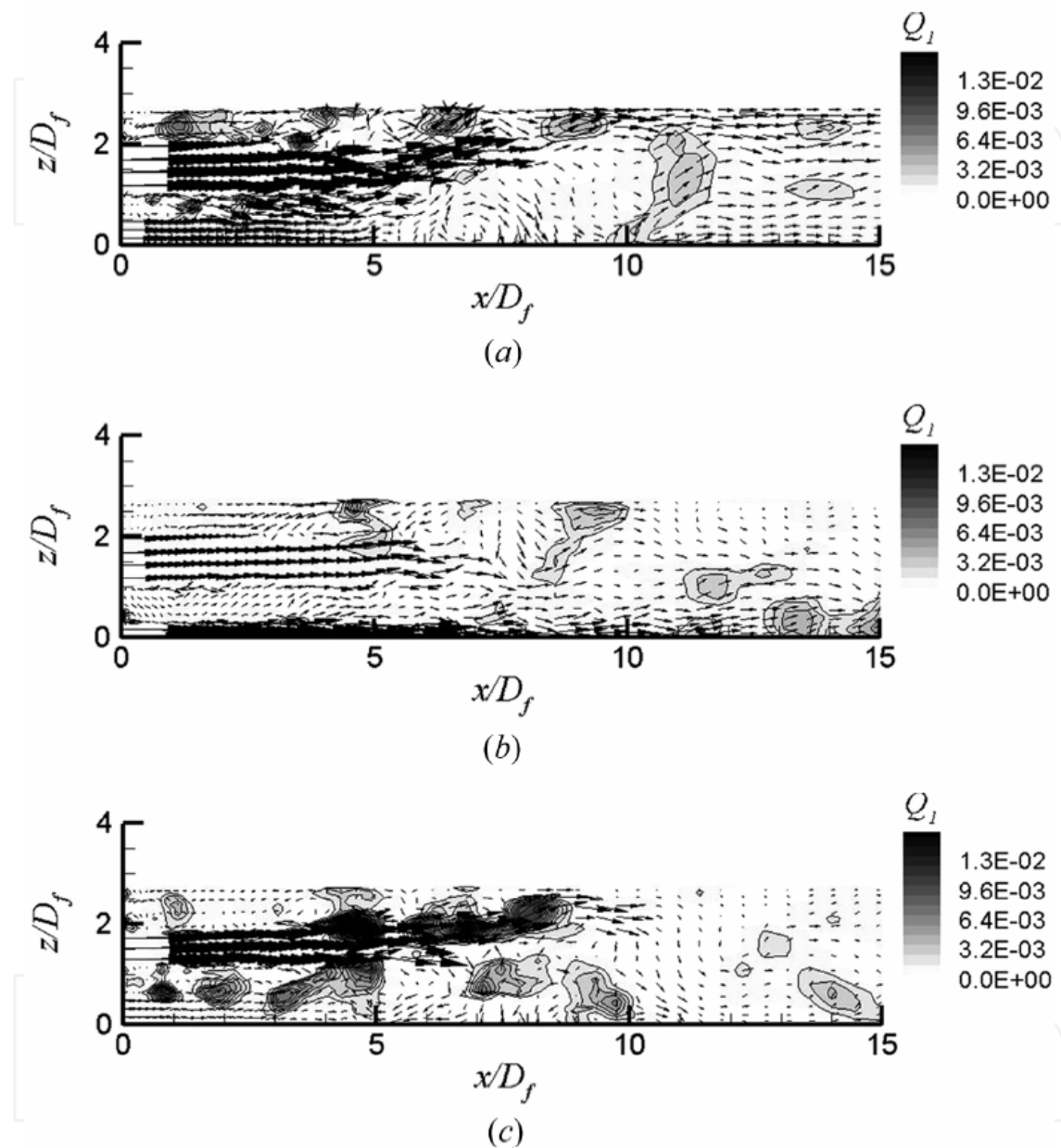

Fig. 12. Instantaneous contour of Q1 and velocity vector fields at (x, z) cross-sectional plane. (a) Case A2; (b) case B; and (c) case C

To show the effect of flow event as a contributor to the wall heat transfer, quadrant analysis is applied to the fluctuating components of velocity and temperature as follows. Figure 12 shows the instantaneous velocity vector fields and Q_1 contour normalized by V_o and Θ_{inlet} for each case, respectively. The Q_1 is defined as $Q_1 = w'\theta'$ when $\theta' > 0$ and $w' > 0$ for (x,z) plane representing hot sweep toward wall or hot wall-ward interaction. For all the three cases, the near-wall recirculation region appears at upstream very close to the wall. However, the central recirculation region is not formed in case B where the velocity ratio is

the lowest as shown in Table 1. For the three cases, the higher Q_1 region is created at the area where strong upward flow exists toward the wall near the reattachment point. In cases A2 and C, the central recirculation region makes the direction of oxidant flow more bent toward the wall and in case C inlet velocity of oxidant jet is the largest. As a result stronger wall-ward hot flow is generated. So, at that region the Q_1 is very high and moreover in case C the level of Q_1 is more raised than the case A2 by virtue of increased wall-ward velocity magnitude. However, in case B, owing to comparatively slow oxidant jet velocity and no augmented wall-ward fluid motion of it caused by the central recirculation region the level of Q_1 near the wall is much decreased. So, the variation of the baffle geometry finally has a great influence on the wall heat transfer and this will be confirmed with heat flux ratio H_j.
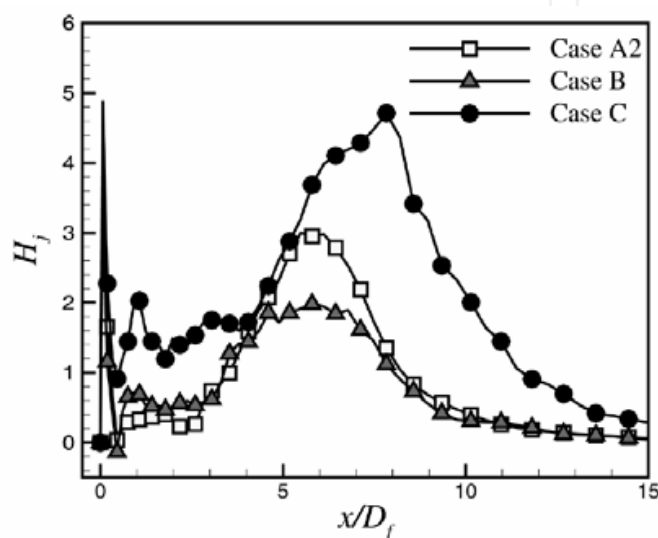

Fig. 13. Distributions of along the streamwise direction

Figure 13 shows the distribution of the heat flux ratio which is averaged for time and space along the circumferential direction at $1.3 < y^+ < 4.0$ very close to the wall. Here the heat flux ratio, H_j, represents the ratio of turbulent heat flux to molecular diffusion near the wall. For all the three cases, the higher magnitude of the heat flux ratio appears at the region of the strong upward flow motion generated by the near-wall flow recirculation region as illustrated in the previous figure. The peak value of the H_j is elevated in the order of the cases B, A2 and C. This indicates that the magnitude of the wall-normal turbulent heat flux is raised with increasing velocity ratio because the strength of the upward fluid motion to the wall is augmented as discussed before. The augmented turbulent heat flux makes the thermal boundary layer thinner resulting in steep temperature gradient near the wall, especially near the reattachment region. It should be noted that the case A2 has the significantly larger H_j values compared with case B only near the reattachment region. Except the reattachment region, the H_j of case B is slightly larger or same as that of the case A2. From the above results, the change of baffle configuration shows different characteristics of heat loss. Consequently, considering the heat loss, the cases A2 and B may be recommended for the micro combustor, but the central recirculation region does not exist in the case B. The central recirculation region greatly helps the mixing between fuel and oxidant and plays an important role for flame holder which becomes much significant in such a small combustor due to relatively larger heat loss. Therefore, the case B is not suitable for the micro combustor and the case A2 is recommended.
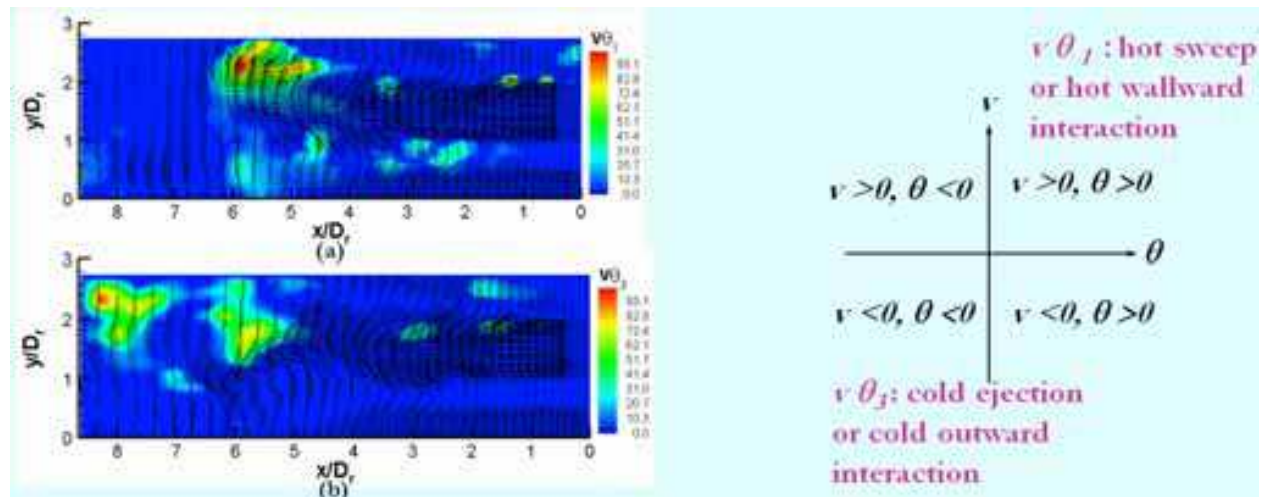
Fig. 14. Contours of instantaneous the 1st and 3rd quadrants of turbulent heat flux and velocity vector map at z=0 plane for case A2

Figure 14 shows contours of instantaneous the 1st and 3rd quadrants of turbulent heat flux and velocity vector map at z=0 plane for case A2. Strong wallward flow is generated inside the instantaneous flow recirculation region and this wallward motion carries hot fluid from the oxidant jet near the combustor wall resulting in a steep temperature gradients there. Cold fluid near the wall is drawn into the central recirculation zone consequently mixed well with hot fluids from fuel jet.
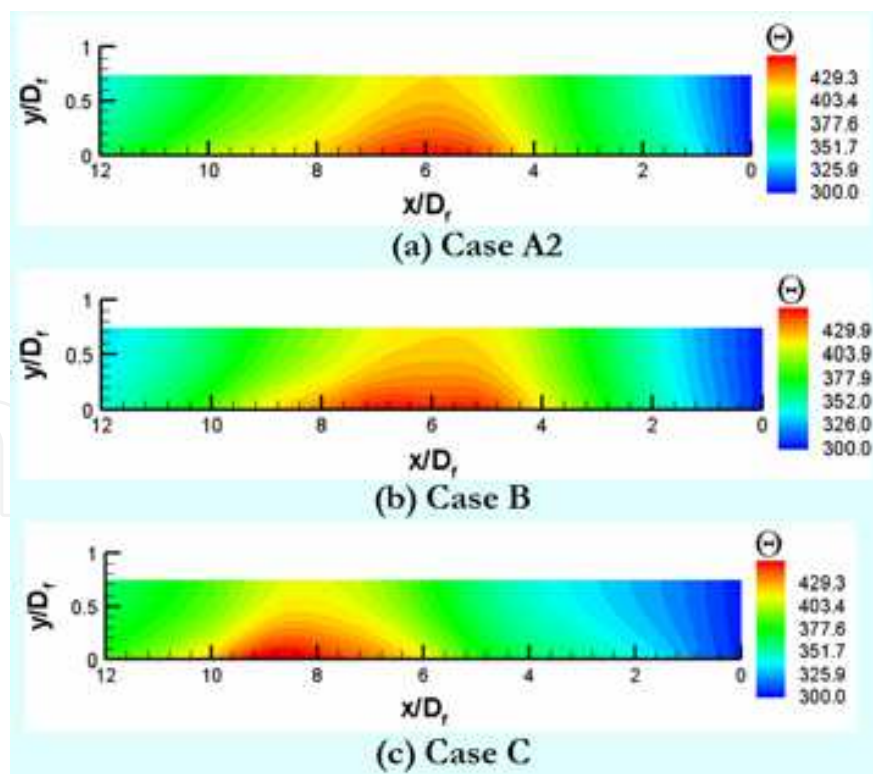

Fig. 15. Temperature distributions of the combustor wall

Figure 15 shows temperature distributions of the combustor wall. For the cases A2 and B, hot regions exist around the middle axial positions. In case C, the hot region is located

further downward axial position compared with cases A2 and B. These phenomena are matched well with the wall Nusselt number distributions. This may decrease the combustion efficiency because of big heat loss from the combustor inside. However, if hot gases are recirculated as in the case of the MGT proposed by (Suzuki et al., 2000), the effect of this heat loss may be mitigated.
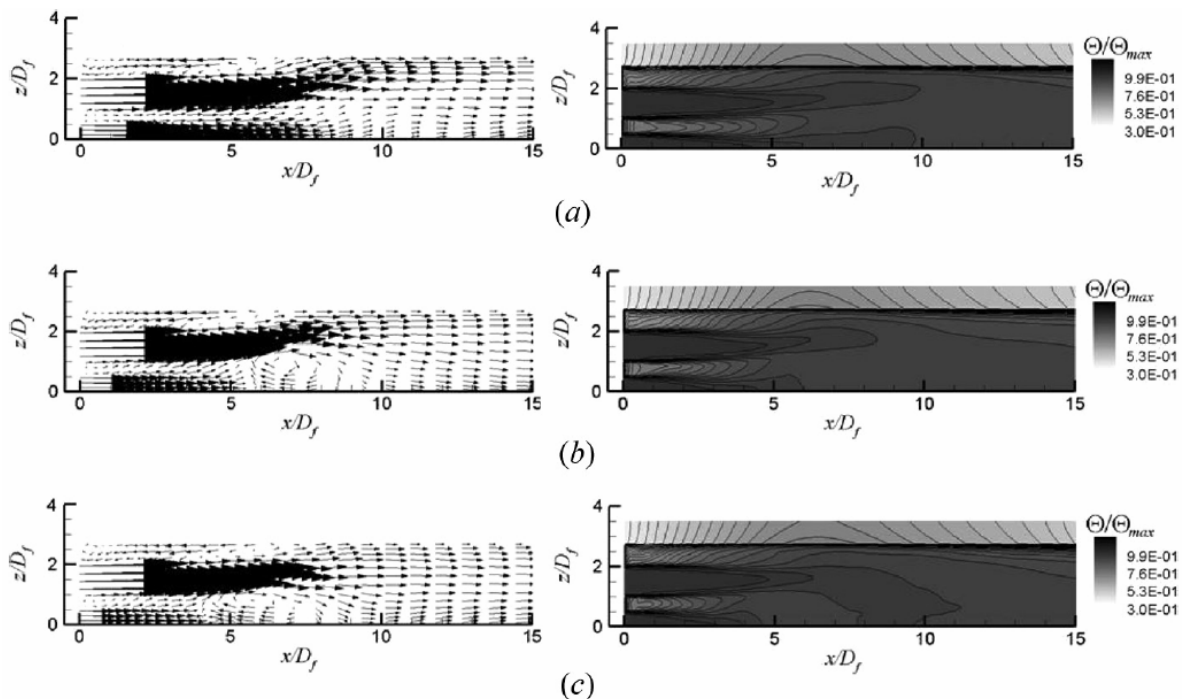

Fig. 16. Contour of Θ/Θmax and velocity vector fields at (x, z) cross-sectional plane. (a) Case A1; (b) case A2; and (c) case A3

To look into the effect of velocity or momentum ratio between fuel jet and oxidant jet flows for the recommended case A2, the cases A1, A2 and A3 are calculated as in Table 1 with the same geometry and similar Reynolds number. Figure 16 shows the contours of time averaged temperature both in the flow field and conjugate wall together with velocity vector fields. With increasing velocity ratio the central recirculation region is generated and the width(streamwise direction) and height(wall-normal direction) of the recirculation region are changed. This greatly affects the evolution of flow and thermal fields. In Figure 16, the near-wall recirculation region exists for the three cases and another tiny recirculation bubble is shown at upstream very close to the baffle plate. In case A1, the path of oxidant jet flow is going toward the wall following streamline of the near-wall recirculation region and at that region close to the wall temperature gradient becomes steep and the temperature gradient of the conjugated wall, too. For cases A2 and A3, the central recirculation region is generated but its configuration is different. In case A2, the central recirculation region looks circular in shape and above it the streamline is curved following it. So, the recirculation region pushes more the oxidant jet flow to upward compared with case A1 and this results in the thinnest thermal boundary layer among the three cases. In case A3 the central recirculation region resembles ellipsoidal shape. Furthermore, according to increased oxidant jet momentum the starting point of the recirculation region appears earlier compared with the case A2. This makes the streamline of the oxidant jet flow partly downward earlier toward the center of

the combustor tube. Therefore, the temperature gradient around $x / D_f = 6$ is the mildest among the three cases.
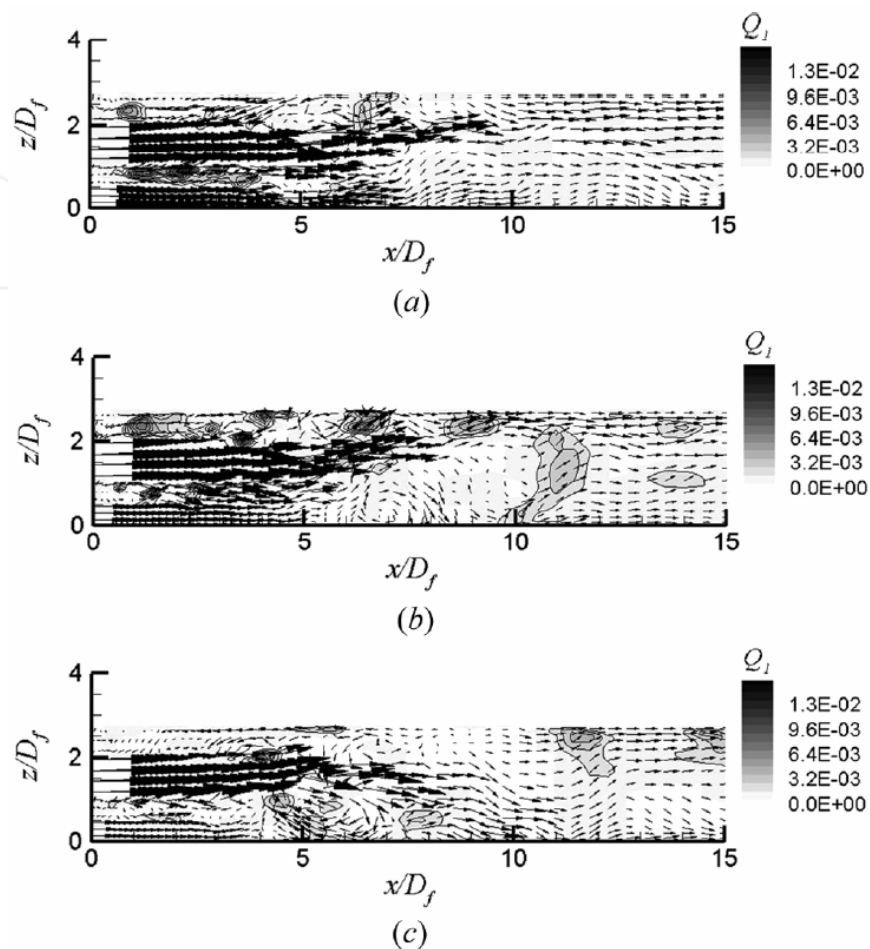

Fig. 17. Instantaneous contour of Q1 and velocity vector fields at (x, z) cross-sectional plane. (a) Case A1; (b) case A2; and (c) case A3

In Figure 17, for all the three cases the instantaneous near-wall recirculation region is generated, but the central flow recirculation region can be shown only in (b) and (c). In case A1, following the outer streamline of the near-wall recirculation region, the oxidant jet is bent toward the wall and the parcels of fuel jet fluids are entrained into the oxidant jet flow because of higher momentum of the oxidant jet. The Q_1 is higher at the regions between fuel and oxidant jets and around the upward flow of the near-wall recirculation region. With increasing velocity ratio in cases (b) and (c), the central recirculation region appears due to smaller fuel jet momentum and this deforms the direction of the oxidant jet flow. In case A2, the velocity of upward flow near the reattachment region is larger than that of case A1 because the passage of oxidant jet becomes narrower by the central flow recirculation region. The larger wall-ward velocity makes Q_1 higher at that region and the level of Q_1 is elevated than that of the region between fuel jet and oxidant jet flows. This makes the thermal boundary layer thinner resulting in steep temperature gradient close to the wall. However, in case A3, the location of the central recirculation region is pulled more upstream because of increased oxidant jet momentum compared with fuel jet one and the shape of the the central recirculation region becomes flatter as ellipsoid. Especially, at this instant of the

case, the direction of oxidant jet is changed toward the center region of the combustor tube. Therefore around the near-wall recirculation region the strength of wall-ward fluid motion is decreased. This results in the reduction of Q_1 at that region. These instantaneous thermal features are repeated and finally have an effect on time-averaged values as discussed before. From the above results, in case of the same baffle plate configuration, the variation of velocity ratio makes the heat loss different in quantity and from this point of view the case A3 might be recommended for a micro combustor.
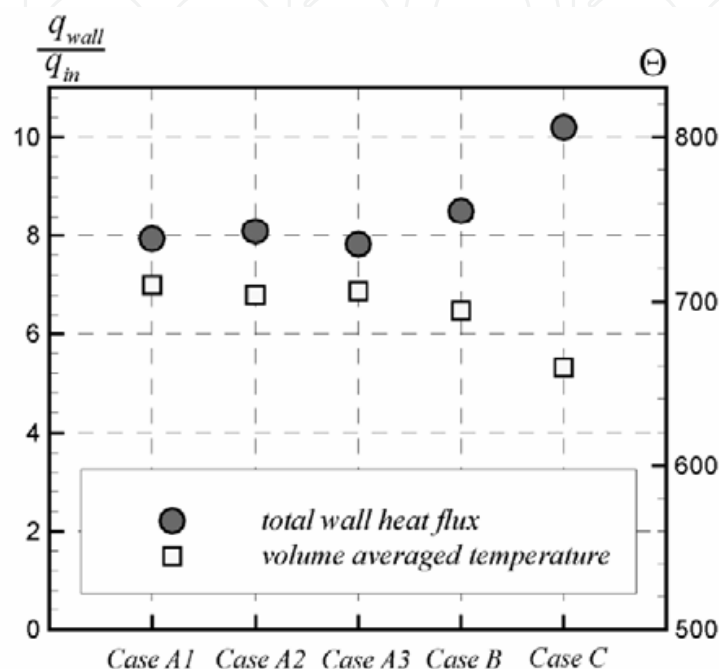

Fig. 18. Comparison of heat loss

Finally, Figure 18 shows the heat loss percentage of the combustor and volume averaged temperature of the fluid for all the cases. Here, the heat loss is defined as the total heat flux passing through the annular wall of the combustor. These are averaged over the combustor wall surface and normalized by heat input. As expected the previous figures, with varying baffle plate shape the total heat loss is increased in the order from the case A2 to B and finally case C. Also, with changing the velocity ratio case A3 has the lowest heat loss. So, the case A3 has the best thermal performance against the heat loss. From the results, for a method to reduce heat loss in the micro combustor, it is recommended that when the near-wall recirculation region exists, its momentum of negative streamwise direction should be decreased. It is noted that the heat generation by combustion should be considered for total thermal energy budget, which is closely connected with mixing efficiency and will be discussed in the future study and from the work of (Choi et al., 2005; Choi et al., 2006a; Choi et al., 2008), the flow recirculation regions can greatly help the mixing enhancement between fuel and oxidant. So, there should be the compromise between mixing enhancement and reduction of heat loss for stable and complete combustion.

4. Conclusion

In this chapter, heat transfer characteristics of multiple jet flows in a micro combustor is investigated by using Large Eddy Simulation (LES). The micro combustor is characterized

by a baffle plate having single fuel nozzle surrounded by six oxidant nozzles annularly and study was made in the three cases of different baffle plate configurations. The baffle plate is mounted to enhance the slow scalar mixing in the low Reynolds number condition of the micro combustor and to hold the flame stable.

With varying baffle plate shapes as the cases of A2, B, and C, the central and near-wall recirculation region appear differently according to the velocity ratio, which is controlled by the configuration and size of the nozzle. In cases with the baffle plates A2 and C, central flow recirculation region is generated and turbulent mixing proceeds more effectively than in the case with the baffle plate B where no central flow recirculation region appears. As a result, mixing is found to be greatly affected by the near-wall flow recirculation regions formed between jets and wall and the central flow recirculation region formed downstream the fuel jet flow. In case C, air jet velocity is high and ring vortices appear most noticeably, intermingling with each other and develop most effectively into turbulent vortices. Also, high momentum of air jet flow brings about the upstream movement of the central flow recirculation region and results in the completion of turbulent mixing within a shorter distance from the baffle plate.

The near-wall recirculation region plays an important role for wall heat transfer, especially near the reattachment region. The central recirculation region only appears in the cases A2 and C and helps turbulent heat transfer to the wall near the reattachment region affecting wall-ward flow. The reattachment flow pushes the hot fluid lumps into the combustor tube wall and this leads to the thinner thermal boundary layer representing higher wall heat transfer there. Among the three cases of different baffle geometry, the case A2 has the smallest wall heat loss, so the case A2 may be recommended for better design of the micro combustor. For this case, to investigate the velocity ratio effect on the same recommended geometry, numerical study is made for the three cases of A1, A2 and A3. With changing the velocity ratio for the cases A1, A2 and A3, the existence and the shape of the central and the near-wall recirculation regions are varied resulting in different heat loss characteristics. Among the three cases, the case A3 shows the minimum heat loss in the present study. It is noted that to prevent the big heat loss, the method of hot gas recirculation by (Suzuki et al., 2000) may be one solution so that the effect of the heat loss may be mitigated.

5. References

Andreopoulos, J. (1993). Heat Transfer Measurement in a Heated Jet-Pipe Flow Issuing into a Cold Cross Stream, *Phys. Fluids*, Vol. 26, pp. 3201-3210, ISSN:1070-6631.

Benard, P. S. & Wallace, J. M. (2002). *Turbulent Flow*, John Willey & Sons Inc., Hoboken, NJ.

Choi, H. S., Nakabe, K., Suzuki K. & Katsumoto, Y. (2001). An Experimental Investigation of Mixing and Combustion Characteristics on the Can-Type Micro Combustor with a Multi-Jet Baffle Plate, *Fluid Mechanics and Its Application*, Vol. 70, pp. 367-375, ISSN:0926-5112.

Choi, H. S., Park, T. S. & Suzuki, K. (2005). LES of Turbulent Flow and Mixing in a Micro Can Combustor, *Proc. 4th Int. Symposium Turbulence and Shear Flow Phenomena*, Vol. 2, pp. 389-394.

Choi, H. S., Park, T. S. & Suzuki, K. (2006a). Numerical Analysis on the Mixing of a Passive Scalar in the Turbulent Flow of a Small Combustor by Using Large Eddy Simulation, *Journal of Computational Fluid Engineering (Korean)*, Vol. 11, pp. 67-74, ISSN:1598-6071.

Choi, H. S., Park, T. S. & Suzuki, K. (2008). Turbulent Mixing of a Passive Scalar in Confined Multiple Jet Flows of a Micro Combustor, *Int. J Heat Mass Transfer*, Vol. 51, pp. 4276-4286, ISSN:0017-9310.

Choi, H. S., Park, T. S. & Suzuki, K. (2006b). Large Eddy Simulation of Turbulent Convective Heat Transfer in a Micro Can Combustor with Multiple Jets, *Proc. 13th Int. Heat Transfer Conference*, Vol. 1, pp. TRB-22.

Choi, H. S. & Park, T. S. (2009). A Numerical Study for Heat Transfer Characteristics of a Micro Combustor by Large Eddy Simulation, *Numerical Heat Trnasfer Part A*, Vol. 56, pp. 230-245, ISSN:1040-7782

Ferziger, J. H. & Peric, M. (2002). *Computational Methods for Fluid Dynamics*, 3rd ed., Springer-Verlag, Berlin, ISBN:3-540-42074-6.

Issa, R. I. (1986). Solution of the Implicitly Discretized Fluid Flow Equations by Operating-Splitting, *J Comput. Phys.*, Vol. 62, pp. 40-65, ISSN:0021-9991.

Kee, R. J., Zhu, H. & Goodwin, D. G. (2005). Solid-Oxide Fuel Cells with Hydrocarbon Fuels, *Proceedings of the Combustion Institute*, Vol. 30, pp. 2379-2404, ISSN:1540-7489.

Le, H., Moin, P. And Kim, J. (1997). Direct Numerical Simulation of Turbulent Flow over a Backward-Facing Step, *J Fluid Mechacnics*, Vol. 330, pp. 349-374.

Lele, S. K. (1992). Compact Finite Difference Schemes with Spectral-Like Resolution, *J Comput. Phys.*, Vol. 103, pp. 16-42, ISSN:0021-9991.

Lilly, D. K. (1992). A Proposed Modification of the Germano Subgrid-Scale Closure Model, *Phys. Fluids*, Vol. 4, pp. 633-635, ISSN:1070-6631.

Massardo, A. F. & Lubelli, F. (2000). Internal Reforming Solid Oxide Fuel Cell-Gas Turbine Combined Cycles(IRSOFCGT) :Part A-Cell Model and Cycle Thermodynamics Analysis, *ASME Journal of Engineering for Gas Turbine and Power*, Vol. 122, pp. 27-35, ISSN:0742-4795.

Mcdonald, C. F. (2000). Low Cost Compact Primary Surface Recuperator Concept for Microturbine, *Applied thermal Engineering*, Vol. 20, pp. 471-497, ISSN:1359-4311.

Moin, P., Squires, K., Cabot, W. & Lee, S. (1991). A Dynamic Subgrid-Scale Model for Compressible Turbulence and Scalar Transport, *Phys. Fluids*, Vol. 3, pp. 2746-2757, ISSN:1070-6631.

Park, T. S. (2006a). Effect of Time-Integration Method in a Large Eddy Simuation using PISO Algorithm: Part I-Flow Field, *Numerical Heat Trnasfer Part A*, Vol. 50, pp. 229-245, ISSN:1040-7782.

Park, T. S. (2006b). Effect of Time-Integration Method in a Large Eddy Simuation using PISO Algorithm: Part II-Thermal Field, *Numerical Heat Trnasfer Part A*, Vol. 50, pp. 247-262, ISSN:1040-7782.

Park, T. S., Sung, H. J. & Suzuki, K. (2003). Development of a Nonlinear Near-Wall Turbulence Model for Turbulent Flow and Heat Transfer, *Int. J Heat Fluid Flow*, Vol. 24, pp. 29-40, ISSN:0142-727X.

Peng, S. H. & Davision, L. (2002). On a Subgrid-Scale Heat Flux Model for Large Eddy Simulation of Turbulent Flow, Stream, *Int. J Heat Mass Transfer*, Vol. 45, pp. 1393-1405, ISSN:0017-9310.

Suzuki, K., Teshima, K. & Kim, J. H. (2000). Solid Oxide Fuel Cell and Micro Gas Turbine Hybrid Cycle for a Distributed Energy Generation System, *Proc. 4th JSME-KSME Thermal Engineering Conference*, Vol. 13, pp. 1-8.
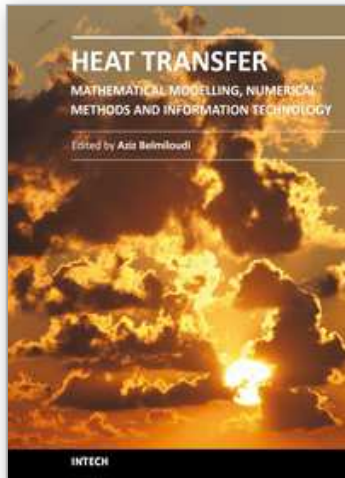
Heat Transfer - Mathematical Modelling, Numerical Methods and Information Technology
Edited by Prof. Aziz Belmiloudi

ISBN 978-953-307-550-1
Hard cover, 642 pages
Publisher InTech
Published online 14, February, 2011
Published in print edition February, 2011

Over the past few decades there has been a prolific increase in research and development in area of heat transfer, heat exchangers and their associated technologies. This book is a collection of current research in the above mentioned areas and describes modelling, numerical methods, simulation and information technology with modern ideas and methods to analyse and enhance heat transfer for single and multiphase systems. The topics considered include various basic concepts of heat transfer, the fundamental modes of heat transfer (namely conduction, convection and radiation), thermophysical properties, computational methodologies, control, stabilization and optimization problems, condensation, boiling and freezing, with many real-world problems and important modern applications. The book is divided in four sections : "Inverse, Stabilization and Optimization Problems", "Numerical Methods and Calculations", "Heat Transfer in Mini/Micro Systems", "Energy Transfer and Solid Materials", and each section discusses various issues, methods and applications in accordance with the subjects. The combination of fundamental approach with many important practical applications of current interest will make this book of interest to researchers, scientists, engineers and graduate students in many disciplines, who make use of mathematical modelling, inverse problems, implementation of recently developed numerical methods in this multidisciplinary field as well as to experimental and theoretical researchers in the field of heat and mass transfer.

How to reference
In order to correctly reference this scholarly work, feel free to copy and paste the following:

Tae Seon Park and Hang Seok Choi (2011). Turbulent Flow and Heat Transfer Characteristics of a Micro Combustor, Heat Transfer - Mathematical Modelling, Numerical Methods and Information Technology, Prof. Aziz Belmiloudi (Ed.), ISBN: 978-953-307-550-1, InTech, Available from:
http://www.intechopen.com/books/heat-transfer-mathematical-modelling-numerical-methods-and-information-technology/turbulent-flow-and-heat-transfer-characteristics-of-a-micro-combustor

INTECH
open science | open minds

www.intechopen.com

Fax: +385 (51) 686 166
www.intechopen.com

Fax: +86-21-62489821